# Towards a gauge-polyvalent numerical relativity code

Daniela Alic, Carles Bona, and Carles Bona-Casas

*Departament de Fisica, Universitat de les Illes Balears, Palma de Mallorca,*
*Spain. Institute for Applied Computation with Community Code (IAC³)0*

The gauge polyvalence of a new numerical code is tested, both in harmonic-coordinate simulations (gauge-waves test bed) and in singularity-avoiding coordinates (simple black-hole simulations, either with or without shift). The code is built upon an adjusted first-order flux-conservative version of the Z4 formalism and a recently proposed family of robust finite-difference high-resolution algorithms. An outstanding result is the long-term evolution (up to $1000M$) of a black hole in normal coordinates (zero shift) without excision.

## I. INTRODUCTION

In a recent paper [1], Kiuchi and Shinkai have analyzed numerically the behavior of many "adjusted" versions of the BaumgarteShapiroShibataNakamura (BSSN) system. This is a follow-up of a former proposal [2] for using the energy-momentum constraints to modify numerical relativity evolution formalisms. An important point was to put the constraint propagation system (subsidiary system) in a strongly-hyperbolic form, so that constraint violations can propagate out of the computational domain. As a further step, there is also the possibility of introducing damping terms, which would attract the numerical solution towards the constrained subspace.

At the first sight, one could wonder why this idea is still deserving some interest today, when the BSSN system is being successfully used in binary-black-holes simulations. Waveform templates are currently being extracted for different mass and spin configurations, with an accuracy level that depends just on the computational resources (including the use of mesh-refinement and/or higher-order finite-difference algorithms). The same is true for neutron stars simulations, where the BSSN formalism is currently used for evolving the spacetime geometry [3–6]. But these success scenarios have a weak point: the BSSN simulations are based on the combination of the "1 + log" and "Gamma-driver" gauge conditions, as proposed in Ref. [7] for the first long-term dynamical simulation of a single black hole (BH) without excision.

Concerning BH simulations, we can understand that dealing numerically with collapse singularities requires the use of either excision, or time slicing prescriptions with strong singularity-avoidance properties. In the '1 + log' case, there is actually a "limit hypersurface", so that the numerical evolution gets safely bounded away from collapse singularities. But singularity-avoidance is a property of the time coordinate, which should then be independent of the space coordinates prescription. In the

spirit of general relativity, we should expect a gauge-polyvalent numerical code to work as well in normal coordinates (zero shift), even if some specific type of time slicing condition (lapse choice) is required for BH simulations. Moreover, this requirement should be extended to other dynamical choices of the space coordinates. This means that a gauge-polyvalent numerical code should also work with alternative shift prescriptions, provided that the proposed choices preserve the regularity of the congruence of time lines. And this should be independent of the fact that a freezing of the dynamics is obtained or not as a result. These considerations apply *a fortriori* to neutron star simulations without any BH in the final stage, where no singularity is expected to form.

The above proposed gauge-polyvalence requirements, which are in keeping with the spirit of general relativity, may seem too ambitious, allowing for the fact that they are not fulfilled by current BH codes. But the need for improvement is even more manifest by looking at the results of the gauge-waves test. This test consists in evolving Minkowsky spacetime in nontrivial harmonic coordinates, and was devised for cross-comparing the numerical codes performance [8]. In Ref. [1], the authors assay different adjustments in order to correct the poor performance of "plain" BSSN codes, which was previously reported in Ref. [9]. They manage to get long-term evolutions for the small amplitude case ($A = 0.01$) with a standard second-order-accurate numerical algorithm. The same result was previously achieved by using a fourth-order accurate finite differences scheme [10]. Even in this case, however, the results for the medium amplitude case ($A = 0.1$) are disappointing. More details can be found in a more recent cross-comparison paper [11], where actually a higher benchmark (big amplitude, $A = 0.5$, devised for testing the nonlinear regime) is proposed.

One could argue that the gauge-waves test is not relevant for real simulations, because periodic boundary conditions do not allow constraint violations to propagate out of the

computational domain [9]. In BH simulations, however, constraint violations arising inside the horizon cannot get out, unless all the characteristic speeds of the subsidiary system are adjusted to be greater than light speed. As far as this extreme adjustment is not implemented in the current evolution formalisms, the gauge-waves test results can be indeed relevant, at least for nonexcision BH codes. As a result, in keeping with the view expressed in Ref. [1], we are convinced that either an improvement of the current BSSN adjustments or any alternative formulation would be welcome, as far as it could contribute to widen the gauge-polyvalence of numerical relativity codes.

In this paper we will consider an alternative numerical code consisting in two main ingredients. The first one is the Z4 strongly-hyperbolic formulation of the field equations [12]. The original (second order) version needs no adjustment for the energy and momentum constraints, as far as constraint deviations propagate with light speed, although some convenient damping terms have been also proposed [13]. We present in Sec. II a first-order version, which has been adjusted for the ordering constraints which arise in the passage from the second-order to the first-order formalism. Its flux-conservative implementation is described in Appendix A. The second ingredient is the recently developed FDOC algorithm [14], which is a (unlimited) finite-difference version of the Osher-Chakrabarthy finite-volume algorithm [15], along the lines sketched in a previous paper [16]. Although this algorithm, detailed in Appendix B, allows a much higher accuracy, we will restrict ourselves here to the simple cases of third and fifth-order accuracy, which have shown an outstanding robustness, confirmed by standard tests from Computational Fluid Dynamics, including multidimensional shock interactions [14].

The results for the gauge-waves test are presented in Sec. III, where just a small amount of dissipation, without any visible dispersion error, shows up after 1000 crossing times, even for the high amplitude $(A = 0.5)$ case. Simulations of a 3D BH in normal coordinates are presented in Sec. IV, where we consider many variants of the "Bona-Massó" singularity-avoidant prescription [17]. As expected, the best results for a given resolution are obtained for the choices with a limit hypersurface far away from the singularity. For the $f = 2/\alpha$ choice, the BH evolves in normal coordinates at least up to $1000M$ in a uniform grid with logarithmic space coordinates. This is one order of magnitude greater than the normal-coordinates BSSN result, as reported in [7].

Concerning the shift conditions, we have tested in Sec. V many explicit first-order prescriptions in single BH simulations. The idea is just to test the gauge-polyvalence of the code, so no physically motivated condition has been imposed, apart from the three-covariance of the shift under arbitrary time-independent coordinate transformations. Our results confirm that the proposed

code is not specially tuned for normal coordinates (zero shift).

## II. ADJUSTING THE FIRST-ORDER Z4 FORMALISM

The Z4 formalism is a covariant extension of the Einstein field equations, defined as [12]

$$R_{\mu\nu} + \nabla_\mu Z_\nu + \nabla_\nu Z_\mu = 8\pi\left(T_{\mu\nu} - \frac{1}{2}Tg_{\mu\nu}\right). \quad (1)$$

The four-vector $Z_\mu$ is an additional dynamical field, which evolution equations can be obtained from (1). The solutions of the original Einstein's equations can be recovered when $Z_\mu$ is a Killing vector. In the generic case, the Killing equation has only the trivial solution $Z_\mu = 0$, so that true Einstein's solutions can be easily recognized.

The manifestly covariant form (1) can be translated into the $3 + 1$ language in the standard way. The covariant four-vector $Z_\mu$ will be decomposed into its space components $Z_i$ and the normal time component

$$\Theta \equiv n_\mu Z^\mu = \alpha Z^0, \quad (2)$$

where $n_\mu$ is the unit normal to the $t =$ constant slices. The $3 + 1$ decomposition of (1) is given then by [12]

$$(\partial_t - \mathcal{L}_\beta)\gamma_{ij} = -2\alpha K_{ij} \quad (3)$$

$$(\partial_t - \mathcal{L}_\beta)K_{ij} = -\nabla_i\alpha_j + \alpha\bigg[R_{ij} + \nabla_i Z_j + \nabla_j Z_i - 2K_{ij}^2$$
$$+ (\text{tr}K - 2\Theta)K_{ij}$$
$$- 8\pi\Big\{S_{ij} - \frac{1}{2}(\text{tr}S - \tau)\gamma_{ij}\Big\}\bigg] \quad (4)$$

$$(\partial_t - \mathcal{L}_\beta)\Theta = \frac{\alpha}{2}[R + 2\nabla_k Z^k + (\text{tr}K - 2\Theta)\text{tr}K$$
$$- \text{tr}(K^2) - 2Z^k\alpha_k/\alpha - 16\pi\tau] \quad (5)$$

$$(\partial_t - \mathcal{L}_\beta)Z_i = \alpha[\nabla_j(K_i{}^j - \delta_i{}^j \text{tr}K) + \partial_i\Theta - 2K_i{}^j Z_j$$
$$- \Theta\alpha_i/\alpha - 8\pi S_i]. \quad (6)$$

The evolution system can be completed by providing suitable evolution equations for the lapse and shift components.

$$\partial_t\alpha = -\alpha^2 Q, \qquad \partial_t\beta^i = -\alpha Q^i. \quad (7)$$

We will keep open at this point the choice of gauge conditions, so that the gauge-derived quantities $\{Q, Q^i\}$ can be either a combination of the other dynamical fields or independent quantities with their own evolution equation. We are assuming, however, that both lapse and shift are dynamical quantities, so that terms involving derivatives of $\{Q, Q^i\}$ actually belong to the principal part of the evolution system.

### A. First-order formulation: ordering constraints

In order to translate the evolution system (3)–(7) into a fully first-order form, the space derivatives of the metric components (including lapse and shift) must be introduced as new independent quantities:

$$A_i \equiv \partial_i \ln\alpha, \qquad B_k{}^i \equiv \partial_k \beta^i, \qquad D_{kij} \equiv \frac{1}{2}\partial_k \gamma_{ij}. \quad (8)$$

Note that, as far as the new quantities will be computed now through their own evolution equations, the original definitions (8) must be considered rather as constraints (first-order constraints), namely

$$\mathcal{A}_k \equiv A_k - \partial_k \ln\alpha = 0 \qquad (9)$$

$$\mathcal{B}_k{}^i \equiv B_k{}^i - \partial_k \beta^i = 0 \qquad (10)$$

$$\mathcal{D}_{kij} \equiv D_{kij} - \frac{1}{2}\partial_k \gamma_{ij} = 0. \qquad (11)$$

Note also that we can derive in this way the following set of constraints, related with the ordering of second derivatives (ordering constraints):

$$\mathcal{C}_{ij} \equiv \partial_i \mathcal{A}_j - \partial_j \mathcal{A}_i = \partial_i A_j - \partial_j A_i = 0, \qquad (12)$$

$$\mathcal{C}_{rs}{}^i \equiv \partial_r \mathcal{B}_s{}^i - \partial_s \mathcal{B}_r{}^i = \partial_r B_s{}^i - \partial_s B_r{}^i = 0, \qquad (13)$$

$$\mathcal{C}_{rsij} \equiv \partial_r \mathcal{D}_{sij} - \partial_s \mathcal{D}_{rij} = \partial_r D_{sij} - \partial_s D_{rij} = 0. \qquad (14)$$

The evolution of the lapse and shift space derivatives could be obtained easily, just by taking the time derivative of the definitions (8) and exchanging the order of time and space derivatives. But then the characteristic lines for the transverse-derivative components in (8) would be the time lines (zero characteristic speed). This can lead to a characteristic degeneracy problem, because the characteristic cones of the second-order system (4)–(6) are basically the light cones [12], and the time lines can actually cross the light cones, as it is the case in many black-hole simulations. In order to avoid this degeneracy problem, we can make use of the shift ordering constraint (13) for obtaining the following evolution equations for the additional quantities (8):

$$\partial_t A_k + \partial_l[-\beta^l A_k + \delta^l{}_k(\alpha Q + \beta^r A_r)] = B_k{}^l A_l - \mathrm{tr}B A_k \qquad (15)$$

$$\partial_t B_k{}^i + \partial_l[-\beta^l B_k{}^i + \delta^l{}_k(\alpha Q^i + \beta^r B_r{}^i)]$$
$$= B_k{}^l B_l{}^i - \mathrm{tr}B B_k{}^i \qquad (16)$$

$$\partial_t D_{kij} + \partial_l[-\beta^l D_{kij} + \delta^l{}_k\{\alpha K_{ij} - 1/2(B_{ij} + B_{ji})\}]$$
$$= B_k{}^l D_{lij} - \mathrm{tr}B D_{kij}. \qquad (17)$$

Note that the characteristic lines for the transverse-derivative components are now the normal lines (instead of the time lines), so that characteristic crossing is actually avoided. This ordering adjustment is crucial for long-term evolution in the dynamical shift case, as it has been yet realized in the first-order version of the generalized-harmonic formulation [18].

### B. Damping terms adjustments

A further adjustment could be the introduction of some constraint-violation damping terms. For the energy-momentum constraints, these terms can be added to the evolution Eqs. (4)–(6), as described in Ref. [13].

For the ordering constraints, we can also introduce simple constraint-violation damping terms when required. For instance, Eq. (15) could be modified as follows:

$$\partial_t A_i + \partial_l[-\beta^l A_i + \delta^l{}_i(\alpha Q + \beta^r A_r)]$$
$$= B_i{}^l A_l - \mathrm{tr}B A_i - \eta \mathcal{A}_i, \qquad (18)$$

with the damping parameter in the range $0 \leq \eta \ll 1/\Delta t$. The same pattern could be applied to Eqs. (16) and (17).

In order to justify this, let us analyze the resulting evolution equations for the first-order constraints (9). Allowing for (15), we would get

$$\partial_t \mathcal{A}_k - \beta^r(\partial_r \mathcal{A}_k - \partial_k \mathcal{A}_r) = \mathcal{B}_k{}^r A_r - \mathcal{B}_r{}^r A_k. \quad (19)$$

The hyperbolicity of the subsidiary evolution Eq. (19) can be analyzed by looking at the normal and transverse components of the principal part along any space direction $\vec{n}$, namely

$$\partial_t \mathcal{A}_n - \beta^\perp(\partial_n \mathcal{A}_\perp) = 0 \qquad (20)$$

$$\partial_t \mathcal{A}_\perp - \beta^n(\partial_n \mathcal{A}_\perp) = 0, \qquad (21)$$

with eigenvalues $(0, -\beta^n)$, which is just weakly hyperbolic in the fully degenerate case, that is for any space direction orthogonal to the shift vector. Note that this is just the subsidiary system governing constraint violations, not the evolution system itself. This means that the main concern here is accuracy, rather than stability. But the resulting (linear) secular growth of first-order constraint violations may become unacceptable in long-term simulations.

These considerations explain the importance of adding constraint-damping terms, so that (15) is replaced by (18). The damping term $-\eta \mathcal{A}_k$ will appear as a result in the subsidiary system also. The linearly growing constraint-violation modes arising from the degenerate coupling in (20) will be kept then under control by these (exponential) damping terms. The same argument applies *mutatis mutandis* to the remaining first-order constraints $\mathcal{B}_k{}^i$, $\mathcal{D}_{kij}$.

### C. Secondary ordering ambiguities

The shift ordering constraints (13) can also be used for modifying the first-order version of the evolution Eq. (6) in

the following way

$$(\partial_t - \mathcal{L}_\beta)Z_i = \alpha[\nabla_j(K_i{}^j - \delta_i{}^j \operatorname{tr} K) + \partial_i\Theta - 2K_i{}^jZ_j$$
$$- \Theta A_i - 8\pi S_i] - \mu(\partial_j B_i{}^j - \partial_i \operatorname{tr} B). \tag{22}$$

Also, the ordering constraints (14) can be used for selecting a specific first-order form for the three-dimensional Ricci tensor appearing in (4) [19]. This can be any combination of the standard Ricci decomposition

$$R_{ij} = \partial_k\Gamma^k{}_{ij} - \partial_i\Gamma^k{}_{kj} + \Gamma^r{}_{rk}\Gamma^k{}_{ij} - \Gamma^k{}_{ri}\Gamma^r{}_{kj} \tag{23}$$

with the De Donder decomposition

$$R_{ij} = -\partial_k D^k{}_{ij} + \partial_{(i}\Gamma_{j)k}{}^k - 2D_r{}^{rk}D_{kij} + 4D^{rs}{}_iD_{rsj}$$
$$- \Gamma_{irs}\Gamma_j{}^{rs} - \Gamma_{rij}\Gamma^{rk}{}_k, \tag{24}$$

which is most commonly used in numerical relativity codes. Following Ref. [19], we will introduce an ordering parameter $\xi$, so that $\xi = 1$ corresponds to the Ricci decomposition (23) and $\xi = -1$ to the De Donder one (24).

The choices of $\mu$ and $\xi$ do not affect the characteristic speeds of the evolution system (see Appendix A for details), nor the structure of the subsidiary system. In this sense, these are rather secondary ordering ambiguities and we will keep these parameters free for the moment, although there are some prescriptions that can be theoretically motivated:

(i) The choice $\mu = 1/2$, $\xi = -1$ allows to recover at the first-order level the equivalence between the generalized-harmonic formulation and (the second-order version of) the Z4 formalism, given by [13]

$$Z^\mu = \frac{1}{2}\Gamma^\mu{}_{\rho\sigma}g^{\rho\sigma} \tag{25}$$

(see Appendix A for more details). This can be important, because the harmonic system is known to be symmetric hyperbolic.

(ii) The choice $\mu = 1$ is the only one that ensures the strong hyperbolicity of the Z3 system, obtained from the Z4 one by setting $\theta = 0$. This can be relevant if we are trying to keep energy-constraint violations close to zero. Allowing for the quasi-equivalence between the Z3 and the BSSN systems [19], this adjustment will affect as well to the first-order version of the BSSN system (NOR system [20]) in simulations using dynamical shift conditions. The same comment applies to the old "Bona-Massó" system [21].

(iii) The choice $\xi = 0$ ensures that the first-order version contains only symmetric combinations of second derivatives of the space metric. This is a standard symmetrization procedure for obtaining a first-order version of a generic second-order equation.

In the numerical simulations in this paper, we have taken $\mu = 1$, $\xi = -1$, although we have also tested other combinations, which also lead to long-term stability.

## III. GAUGE WAVES TEST

We will begin with a test devised for harmonic coordinates. Let us consider the following line element:

$$ds^2 = H(x - t)(-dt^2 + dx^2) + dy^2 + dz^2, \tag{26}$$

where $H$ is an arbitrary function of its argument. One could naively interpret this as the propagation of an arbitrary wave profile with unit speed. But it is a pure gauge effect, because (26) is nothing but the Minkowsky metric, written in some nontrivial harmonic coordinates system.

As proposed in Refs. [8,11], we will consider the "gauge waves" line element (26), with the following profile:

$$H = 1 - A\sin(2\pi(x - t)), \tag{27}$$

so that the resulting metric is periodic and we can identify for instance the points $-0.5$ and $0.5$ on the $x$ axis. This allows to set up periodic boundary conditions in numerical simulations, so that the initial profile keeps turning around along the $x$ direction. One can in this way test the long-term effect of these gauge perturbations. The results show that the linear regime (small amplitude, $A = 0.01$) poses no serious challenge to most numerical relativity codes (but see Ref. [1] for the BSSN case). Following the recent suggestion in Ref. [11], we will then focus in the medium and big amplitude cases ($A = 0.1$ and $A = 0.5$, respectively), in order to test the non-linear regime. Concerning grid spacing, although $\Delta x = 0.01$ would be enough for passing the test in the medium amplitude case, the big amplitude one requires more resolution, so we have taken $\Delta x = 0.005$ in both cases.

The results of the numerical simulations are displayed in Fig. 1 for the $H$ function (the $\gamma_{xx}$ metric component). The left panel shows the medium amplitude case $A = 0.1$. Only a small amount of numerical dissipation is barely visible after 1000 round trips: the third-order-accurate finite-difference method gets rid of the dominant dispersion error. For comparison, let us recall that the corresponding BSSN simulation crashes before 100 round trips [10]. The right panel shows the same thing for the large amplitude case $A = 0.5$, well inside the nonlinear regime. We see some amplitude damping, together with a slight decrease of the mean value of the lapse.

Our results are at the same quality level than the ones reported in Ref. [11] for the flux-conservative generalized-harmonic code Abigail (see also the "apples with apples" webpage [22]), which is remarkable for a test running in strictly harmonic coordinates. We can also compare with the simulations reported in Ref. [23] for (a specific variant of) the KST evolution system [24]. Although the gauge-wave parametrization is not the standard one, both their "big amplitude" case and their finest resolution are similar
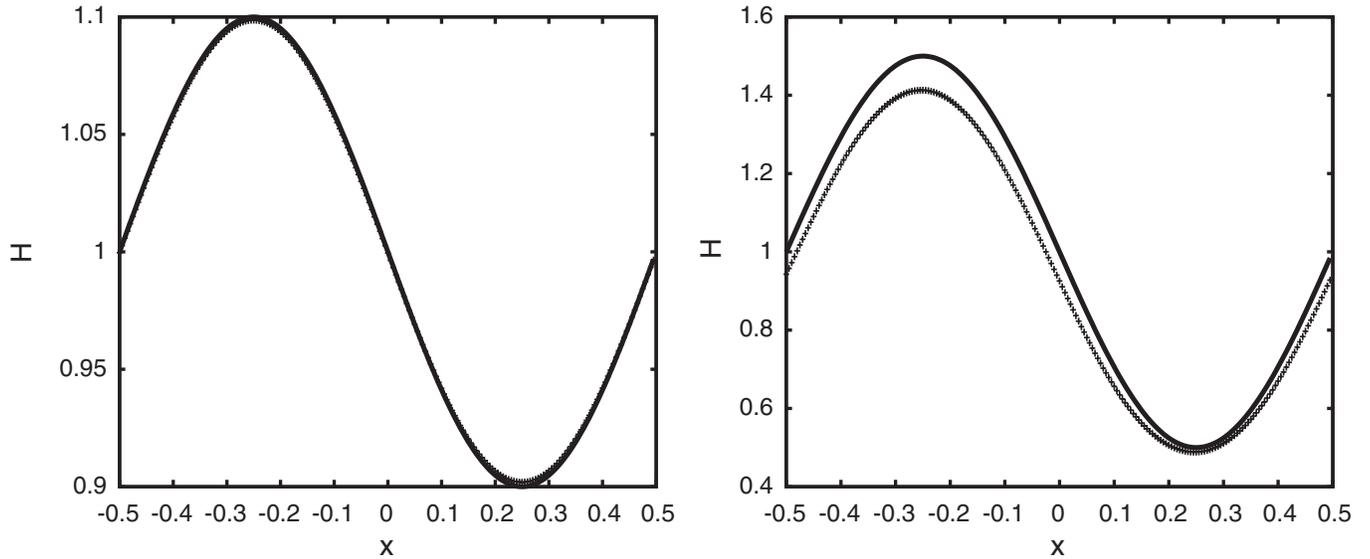
FIG. 1.   Gauge waves simulation with periodic boundary conditions and sinusoidal initial data for the $\gamma_{xx}$ metric component. The resolution is $\Delta x = 0.005$ in both cases. The left panel corresponds to the medium amplitude case $A = 0.1$. After 1000 round trips, the evolved profile (cross marks) nearly overlaps the initial one (continuous line), which corresponds also with the exact solution. The right panel corresponds to the same simulation for the big amplitude case $A = 0.5$. We see the combination of a slight decrease in the mean value plus some amplitude damping.

to ours. We see a clear phase shift, due to cumulative dispersion errors, after about 500 crossing times. We see also a growing amplitude mode, which can be moderated with resolution (for the finest one, it just compensates numerical dissipation). This can be related with the spurious linear mode that has been reported for harmonic systems which are not written in flux-conservative form [8].

We can conclude that there are two specific ingredients in our code that contribute to the gauge-wave results in an essential way: the flux-conservative form of the equations (see Appendix A), which gets rid of the spurious growing amplitude modes, and the third-order accuracy of the numerical algorithm, which reduces the dispersion error below the visual detection level in Fig. 1, even after 1000 crossing times.

## IV. SINGLE BLACK HOLE TEST: NORMAL COORDINATES

We will try next to test a Schwarzschild black-hole evolution in normal coordinates (zero shift). Harmonic codes are not devised for this gauge choice, so we will compare with BSSN results instead. Concerning the time coordinate condition, our choice will be limited by the singularity-avoidance requirement, as far as we are not going to excise the black-hole interior. Allowing for these considerations, we will determine the gauge evolution Eqs. (7) as follows

$$Q = f(\text{tr}K - m\Theta), \qquad Q^i = 0 \qquad (\beta^i = 0), \quad (28)$$

where the second gauge parameter $m$ is a feature of the Z4

formalism. We will choose here by default $m = 2$, because the evolution equation for the combination $\text{tr}K - 2\Theta$, as derived from (4) and (5), actually corresponds with the BSSN evolution equation for $\text{tr}K$ (see Ref. [19] for the relationship between BSSN and Z4 formalisms).

Concerning the first gauge parameter, we will consider first the $1 + \log$ choice $f = 2/\alpha$ [25], which is the one used in current binary BH simulations in the BSSN formalism. The name comes from the resulting form of the lapse, after integrating the evolution Eqs. (3) and (7) with the prescription (28) for true Einstein's solutions ($\Theta = 0$):

$$\alpha = \alpha_0 + \ln(\gamma/\gamma_0), \qquad (29)$$

where $\sqrt{\gamma}$ is the space volume element. It follows from (29) that the coordinate time evolution stops at some limit hypersurface, before even getting close to the collapse singularity. This happens when

$$\sqrt{\gamma/\gamma_0} = \exp(-\alpha_0/2), \qquad (30)$$

that is well before the vanishing of the space volume element: the initial lapse value is usually close to 1, so that the final volume element is still about a 60% of the initial one. This can explain the robustness of the $1 + \log$ choice in current black-hole simulations.

We will consider as usual initial data on a time-symmetric time slice ($K_{ij} = 0$) with the intrinsic metric given in isotropic coordinates:

$$\gamma_{ij} = \left(1 + \frac{m}{2r}\right)^4 \delta_{ij}. \qquad (31)$$

This is the usual "puncture" metric, with the apparent horizon at $r = m/2$: the interior region is isometric to the exterior one, so that the $r = 0$ singularity is actually the image of space infinity. We prefer, however, to deal with nonsingular initial data. We will then replace the constant mass profile in interior region $r < M/2$ by a suitable profile $m(r)$, so that the interior metric corresponds to a scalar field matter content. Of course, the scalar field itself must be evolved consistently there (see Appendix C for details). A previous implementation of the same idea, with dust interior metrics, can be found in Ref. [26].

We have performed a numerical simulation for the $f = 2/\alpha$ case with a uniform grid with resolution $h = 0.1M$, extending up to $r = 20M$ (no mesh-refinement). We have used the third and fifth-order FDOC algorithms, as described in Appendix B, with the optimal dissipation parameters for each case. The results for the lapse profile are shown in Fig. 2 at $t = 20M$ an $t = 40M$. We see in both cases that the higher-order algorithm leads to steeper profiles and a slower propagation of the collapse front. Note that the differences in the front propagation speed keep growing in time, although the third-order plot at $t = 40M$ is clearly affected by the vicinity of the outer boundary. This fact does not affect the code stability, as far as we can proceed with the simulations beyond $t = 50M$, when the collapse front gets out of the computational domain (beyond $t = 60M$ in the higher-order simulations). Note that the corresponding BSSN simulations ($f = 2/\alpha$ in normal coordinates) are reported to crash at about $t = 40M$ [7].
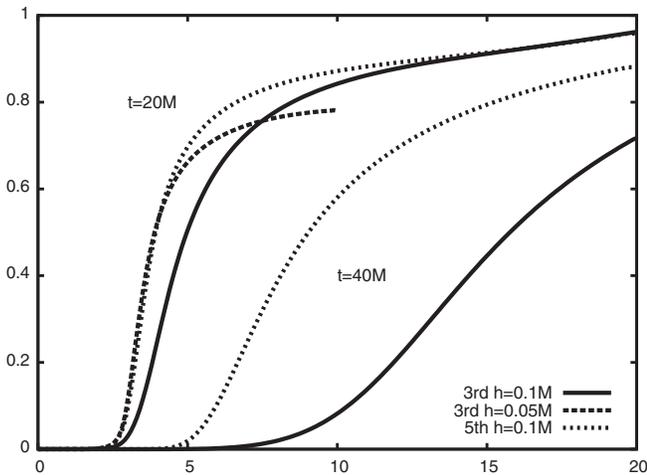


FIG. 2. Plots of the lapse profiles at $t = 20M$ and $t = 40M$. The results for the third-order accurate algorithm (continuous lines) are compared with those for the fifth-order algorithm (dotted lines) for the same resolution ($h = 0.1M$). We have also included for comparison one extra line, corresponding to the third-order results with $h = 0.05M$, computed in a reduced mesh. Increasing resolution leads to a slope steepening and a slower propagation of the collapse front. In this sense, as we can see for $t = 20M$, switching to the fifth-order algorithm while keeping $h = 0.1M$ amounts to doubling the resolution for the third-order algorithm.

TABLE I. Different prescriptions for the gauge parameter $f$, with the corresponding values of the residual volume element at the limit surface (normal coordinates), assuming a unit value of the initial lapse.

| $f$ | $2/\alpha$ | $1 + 1/\alpha$ | $1/2 + 1/\alpha$ | $1/\alpha$ |
|---|---|---|---|---|
| $\sqrt{\gamma/\gamma_0}$ | 61% | 50% | 44% | 37% |

We have added for comparison an extra plot in Fig. 2, with the results at $t = 20M$ of a third-order simulation with double resolution ($h = 0.05M$), obtained in a smaller computational domain (extending up to $10M$). Both the position and the slope of the collapse front coincide with those of the fifth-order algorithm with $h = 0.1M$. In this case, switching to the higher-order algorithm amounts to doubling accuracy. Note, however, that higher-order algorithms are known to be less robust [14]. Moreover, as the profiles steepen, the risk of under-resolution at the collapse front increases. We have found that a fifth-order algorithm is a convenient trade-off for our $h = 0.1M$ resolution in isotropic coordinates.

We have also explored other slicing prescriptions with limit surfaces closer to the singularity, as described in Table I. Note that in these cases the collapse front gets steeper than the one shown in Fig. 2 for the standard $f = 2/\alpha$ case with the same resolution. This poses an extra challenge to numerical algorithms, so we have switched to the third-order-accurate one for the sake of robustness. In all cases, the simulations reached $t = 50M$ without problem, meaning that the collapse front has get out of the computational domain. It follows that the standard prescription $f = 2/\alpha$, although it leads actually to smoother profiles, is not crucial for code stability.

The results shown in Fig. 2 compare with the ones in Ref. [27], obtained with (a second-order version of) the old Bona-Massó formalism. We see the same kind of steep profiles, produced by the well-known slice-stretching mechanism [28]. This poses a challenge to standard numerical methods: in Ref. [27] Finite-Volume methods where used, including slope limiters. Our FDOC algorithm (see Ref. [14] for details) can also be interpreted as an efficient Finite-Differences (unlimited) version of the Osher-Chakrabarthy Finite-Volume algorithm [15]. Note however that in Ref. [27], like in the BSSN case, a conformal decomposition of the space metric was considered, and an spurious (numerical) trace mode arise in the trace-free part of the extrinsic curvature. An additional mechanism for resetting this trace to zero was actually required for stability. In our (first-order) Z4 simulations, both the plain space metric and extrinsic curvature can be used directly instead, without requiring any such trace-cleaning mechanisms.

Let us take one further step. Note that the lifetime of our isotropic coordinates simulations (with no shift) is clearly limited by the vicinity of the boundary (at $r = 20M$). At
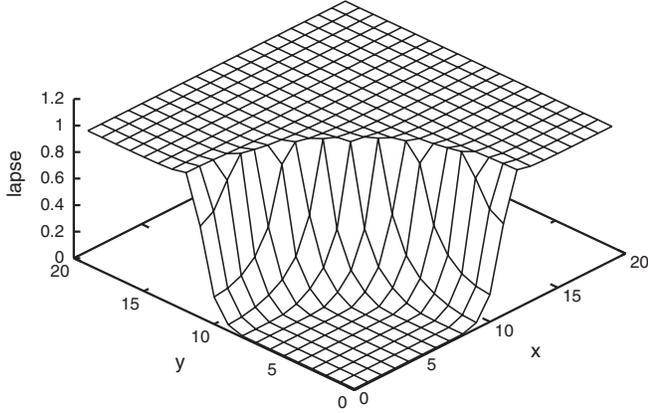
FIG. 3.   Plot of the lapse function for a single BH at $t = 1000M$ in normal coordinates. Only one of every ten points is shown along each direction. The third-order accurate algorithm has been used with $\beta = 1/12$ and a space resolution $h = 0.1M$. The profile is steep, but smooth: no sign of instability appears. Small riddles, barely visible on the top of the collapse front, signal some lack of resolution because of the logarithmic character of the grid. The dynamical zone is safely away from the boundaries.

this point, we can appeal to space coordinates freedom, switching to some logarithmic coordinates, as defined by

$$R = L \sinh(r/L), \tag{32}$$

where $R$ is the new radial coordinate and $L$ some length scale factor. This configuration suggests using the third-order algorithm because of its higher robustness. We have performed a long-term numerical simulation for the $f = 2/\alpha$ case, with $L = 1.5M$, so that $R = 20M$ in these logarithmic coordinates corresponds to about $r = 463.000M$ in the original isotropic coordinates. In this way, as shown in Fig. 3, the collapse front is safely away from the boundary, even at very late times. We stopped our code at $t = 1000M$, without any sign of instability. This provides a new benchmark for Numerical Relativity codes: a long-term simulation of a single black-hole, without excision, in normal coordinates (zero shift). Moreover, it shows that a nontrivial shift prescription is not a requisite for code stability in BH simulations.

## V. SINGLE BLACK HOLE TEST: FIRST-ORDER SHIFT CONDITIONS

Looking at the results of the previous section, one can wonder wether our code is just tuned for normal coordinates. This is why we will consider here again BH simulations, but this time with some nontrivial shift prescriptions. The idea is just to test some simple cases in order to show the gauge-polyvalence of the code. For the sake of simplicity, we will consider here just first-order shift prescriptions, meaning that the source terms $(Q, Q^i)$ in the gauge evolutions (7) are algebraic combinations of

the remaining dynamical fields. To be more specific, we shall keep considering slicing conditions defined by

$$Q = -\beta^k/\alpha A_k + f(\mathrm{tr}K - m\Theta), \tag{33}$$

together with dynamical shift prescriptions, defined by different choices of $Q^i$.

First-order shift prescriptions have been yet considered at the theoretical level [29]. We will introduce here an additional requirement, which follows when realizing that, allowing for the $3 + 1$ decomposition of the line element

$$ds^2 = -\alpha^2 dt^2 + \gamma_{ij}(dx^i + \beta^i dt)(dx^j + \beta^j dt), \tag{34}$$

the shift behaves as a vector under (time independent) transformations of the space coordinates. We will impose then that its evolution equation, and then $Q^i$, is also three-covariant.

This three-covariance requirement could seem a trivial one. But note that the harmonic shift conditions, derived from

$$\Box x^i = 0, \tag{35}$$

are not three-covariant (the box here stands for the wave operator acting on scalars). In the $3 + 1$ language, (35) can be translated as

$$\partial_t(\sqrt{\gamma}/\alpha \beta^i) - \partial_k(\sqrt{\gamma}/\alpha \beta^k \beta^i) + \partial_k(\alpha \sqrt{\gamma} \gamma^{ik}) = 0, \tag{36}$$

where the noncovariance comes from the space-derivatives terms.

Concerning the advection term, a three-covariant alternative would be provided either by the Lie-derivative term

$$\mathcal{L}_\beta(\sqrt{\gamma}\beta^i/\alpha) = \mathcal{L}_\beta(\sqrt{\gamma}/\alpha)\beta^i, \tag{37}$$

or by the three-covariant derivative term

$$\beta^k \nabla_k(\beta^i/\alpha) = 1/\alpha[\beta^k B_k{}^i - \beta^i \beta^k A_k + \Gamma^i_{jk}\beta^j\beta^k]. \tag{38}$$

We have tested both cases in our numerical simulations.

Concerning the last term in (36), we can take any combination of $A^i$, $Z^i$ and the vectors obtained form the space metric derivatives after subtracting their initial values, namely:

$$D_i - D_i|_{t=0}, \qquad E_i - E_i|_{t=0}. \tag{39}$$

This is because the additional terms arising in the transformation of the noncovariant quantities $(D_i, E_i)$ depend only on the space coordinates transformation, which is assumed to be time-independent. Note that, for the conformal contracted-Gamma combination

$$\Gamma_i = 2E_i - \frac{2}{3}D_i, \tag{40}$$

the subtracted terms actually vanish in simulations starting from the isotropic initial metric (31). Of course, the same

remark applies to the BSSN Gamma quantity, namely [19]

$$\tilde{\Gamma}_i = \Gamma_i + 2Z_i. \tag{41}$$

We have considered the following combinations:

$$S1: \partial_t \beta^i = \frac{\alpha^2}{2} A^i - \alpha Q \beta^i \tag{42}$$

$$S2: \partial_t \beta^i = \frac{\alpha^2}{2} A^i + \beta^k B_k{}^i + \Gamma^i_{jk} \beta^j \beta^k - \alpha Q \beta^i \tag{43}$$

$$S3: \partial_t \beta^i = \frac{\alpha^2}{4} \tilde{\Gamma}^i + \beta^k B_k{}^i + \Gamma^i_{jk} \beta^j \beta^k - \alpha Q \beta^i, \tag{44}$$

where S1 corresponds to the Lie-derivative term (37) and the remaining two choices to the covariant advection term (38), with different combinations of the first-order vector fields.

We have obtained stable evolution in all cases, with the simulations lasting up to the point when the collapse front crosses the outer boundary (about $t = 50M$). We can see in Fig. 4 the lapse and shift profiles in the S1 and the S3 cases (S2 is very similar to S1). The shift profiles are modulated by the lapse ones, so that the shift goes to zero in the collapsed regions. This is a consequence of the term $-\alpha Q \beta^i$ in the shift evolution equation, devised for getting finite values of the combination $\beta^i/\alpha$. In the noncollapsed region, S1 leads to a higher shift profile, which spreads out with time, whereas S3 leads to a lower profile, which starts diminishing after the initial growing. Allowing for (44),

this indicates that the conformal gamma quantity $\tilde{\Gamma}_i$ is driven to zero. The lapse slopes are also slightly softened in the S3 case.

These results confirm that the code stability is not linked to any particular shift prescription, as we can combine different source terms in the shift evolution equation, leading to different lapse and shift profiles.

## VI. CONCLUSIONS AND OUTLOOK

We have shown in this paper how a first-order flux-conservative version of the Z4 formalism can be adjusted for dealing with the ordering constraints, and then implemented in a numerical code by means of a robust, cost-efficient, finite-difference formula. The resulting scheme has been tested in a demanding harmonic-coordinates scenario: the gauge-waves test bed. The code performance compares well with the best harmonic-code results for this test [11], even in the highly nonlinear regime (50% amplitude case). This is in contrast with the well-known problems of BSSN-based codes with the gauge-waves test [1,8].

The code has also been tested in nonexcision BH evolutions, where singularity-avoidance is a requirement. Our results confirm the robustness of the code for many different choices of dynamical lapse and shift prescriptions. In the normal coordinates case (zero shift), our results set up a new benchmark, by evolving the BH up to $1000M$ without any sign of instability. This improves the reported BSSN result by one order of magnitude (Harmonic codes are not devised for normal coordinates). More important, this shows that a specific shift choice is not crucial for code stability, even in nonexcision BH simulations. This is confirmed by our shift simulations, where different covariant
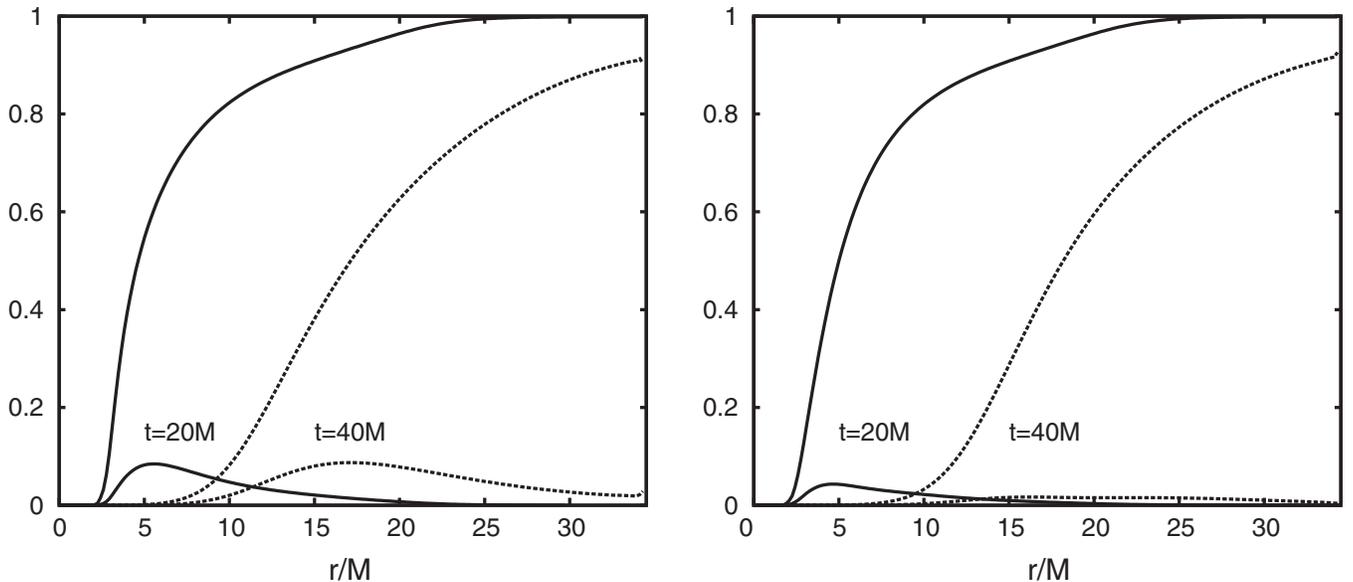


FIG. 4. Plot of the lapse and shift profiles at $t = 20M$ (continuous lines) and $t = 40M$ (dotted lines). The plots are shown along the main diagonal of the computational domain, in order to keep the outer boundary out of the dynamical zone. In the S1 case (left panel), after the initial growing, the maximum shift value keeps constant. In the S3 case (right panel), it clearly diminishes with time.

evolution equations for the shift lead also to stable numerical evolution.

In spite of the encouraging performance in these basic tests, we still are on the way towards a gauge-polyvalent code, as pointed out by the title of this paper. More technical developments on the numerical part are required: mesh refinement, improved boundary treatment, etc. On the theoretical side, as far as the shift prescription is no longer determined by numerical stability, we can explore shift choices from the physical point of view, adapting our space coordinates system to the features of every particular problem. We are currently working in these directions.

## ACKNOWLEDGMENTS

## APPENDIX A: FLUX-CONSERVATIVE EVOLUTION EQUATIONS

We will write the first-order evolution system in a balance-law form. For a generic quantity $u$, this leads to

$$\partial_t u + \partial_k F^k(u) = S(u), \tag{A1}$$

where the flux $F^k(u)$ and source terms $S(u)$ can depend on the full set of dynamical fields in an algebraic way. In the case of the space-derivatives fields, their evolution Eqs. (15)–(17) are yet in the balance-law form (A1). Note however that any damping terms of the form described in (18) will contribute both to the flux and the source terms in a simple way.

The metric evolution Eq. (3) will be written in the form

$$\partial_t \gamma_{ij} = 2\beta^k D_{kij} + B_{ij} + B_{ji} - 2\alpha K_{ij}, \tag{A2}$$

so that it is free of any flux terms. The remaining (nontrivial) evolution Eqs. (4)–(6) require a more detailed development. We will expand first the flux terms in the following way:

$$\partial_t K_{ij} + \partial_k [-\beta^k K_{ij} + \alpha \lambda^k{}_{ij}] = S(K_{ij}) \tag{A3}$$

$$\partial_t Z_i + \partial_k [-\beta^k Z_i + \alpha \{-K^k{}_i + \delta^k{}_i (\mathrm{tr}K - \Theta)\} + \mu(B_i{}^k - \delta_i{}^k \mathrm{tr}B)] = S(Z_i) \tag{A4}$$

$$\partial_t \Theta + \partial_k [-\beta^k \Theta + \alpha(D^k - E^k - Z^k)] = S(\Theta) \tag{A5}$$

where we have used the shortcuts $D_i \equiv D_{ik}{}^k$ and $E_i \equiv D^k{}_{ki}$, and

$$\lambda^k{}_{ij} = D^k{}_{ij} - \frac{1}{2}(1 + \xi)(D_{ij}{}^k + D_{ji}{}^k)$$
$$+ \frac{1}{2}\delta^k{}_i [A_j + D_j - (1 - \xi)E_j - 2Z_j]$$
$$+ \frac{1}{2}\delta^k{}_j [A_i + D_i - (1 - \xi)E_i - 2Z_i]. \tag{A6}$$

The source terms $S(u)$ do not belong to the principal part and will be displayed later. Let us focus for the moment in the hyperbolicity analysis, by selecting a specific space direction $\vec{n}$, so that the corresponding characteristic matrix is

$$A^n = \frac{\partial F^n}{\partial u}, \tag{A7}$$

where the symbol $n$ replacing an index stands for the projection along the selected direction $\vec{n}$. We can get by inspection the following (partial) set of eigenfields, independently of the gauge choice:

(i) *Transverse derivatives*:

$$A_\perp, \qquad B_\perp{}^i, \qquad D_{\perp ij}, \tag{A8}$$

propagating along the normal lines (characteristic speed $-\beta^n$). The symbol $\perp$ replacing an index means the projection orthogonal to $\vec{n}$.

(ii) *Light-cone eigenfields*, given by the pairs

$$F^n[D_{n\perp\perp}] \pm F^n[K_{\perp\perp}] \tag{A9}$$

$$- F^n[Z_\perp] \pm F^n[K_{n\perp}] \tag{A10}$$

$$F^n[D_n - E_n - Z_n] \pm F^n[\Theta] \tag{A11}$$

with characteristic speed $-\beta^n \pm \alpha$, respectively.

Note that the eigenvector expressions given above, in terms of the fluxes, are valid for any choice of the ordering parameters $\mu$ and $\xi$. Only the detailed expression of the eigenvectors, obtained from the flux definitions, is affected by these parameter choices. For instance

$$F^n[D_n - E_n - Z_n] = -\beta^n [D_n - E_n - Z_n]$$
$$+ \alpha\theta + (\mu - 1)\mathrm{tr}(B_{\perp\perp}). \tag{A12}$$

Any value $\mu \neq 1$ implies that the characteristic matrix of the Z3 system, obtained by removing the variable $\theta$ from our Z4 evolution system [19], cannot be fully diagonalized in the dynamical shift case. Of course, the hyperbolicity analysis cannot be completed until we get suitable coordinate conditions, amounting to some prescription for the lapse and shift sources $Q$ and $Q_i$, respectively. But the subset of eigenvectors given here is gauge independent: nondiagonal blocs cannot be fixed *a posteriori* by the coordinates choice.

The detailed expressions for the eigenvectors can be relevant when trying to compare with related formulations. For instance, a straightforward calculation shows that the eigenvectors (A9)–(A11) can be matched to the corre-

sponding ones in the harmonic formalism if and only if

$$\xi = -1, \qquad \mu = 1/2. \tag{A13}$$

This shows that different requirements can point to different choices of these ordering parameters. We prefer then

to leave this choice open for future applications. Concerning the simulations in this paper, we have taken $\xi = -1$, $\mu = 1$.

Finally, we give for completeness the source terms, namely:

$$
\begin{aligned}
S(K_{ij}) = & -K_{ij}\,\mathrm{tr}B + K_{ik}B_j{}^k + K_{jk}B_i{}^k + \alpha\Big\{\frac{1}{2}(1+\xi)\Big[-A_k\Gamma^k{}_{ij} + \frac{1}{2}(A_iD_j + A_jD_i)\Big] \\
& + \frac{1}{2}(1-\xi)\Big[A_kD^k{}_{ij} - \frac{1}{2}\{A_j(2E_i - D_i) + A_i(2E_j - D_j)\} + 2(D_{ir}{}^m D^r{}_{mj} + D_{jr}{}^m D^r{}_{mi}) - 2E_k(D_{ij}{}^k + D_{ji}{}^k)\Big] \\
& + (D_k + A_k - 2Z_k)\Gamma^k{}_{ij} - \Gamma^k{}_{mj}\Gamma^m{}_{ki} - (A_iZ_j + A_jZ_i) - 2K^k{}_iK_{kj} + (\mathrm{tr}K - 2\Theta)K_{ij}\Big\} \\
& - 8\pi\alpha\Big[S_{ij} - \frac{1}{2}(\mathrm{tr}S - \tau)\gamma_{ij}\Big]
\end{aligned}
\tag{A14}
$$

$$
S(Z_i) = -Z_i\,\mathrm{tr}B + Z_kB_i{}^k + \alpha[A_i(\mathrm{tr}K - 2\Theta) - A_kK^k{}_i - K^k{}_r\Gamma^r{}_{ki} + K^k{}_i(D_k - 2Z_k)] - 8\pi\alpha S_i \tag{A15}
$$

$$
S(\Theta) = -\Theta\,\mathrm{tr}B + \frac{\alpha}{2}[2A_k(D^k - E^k - 2Z^k) + D_k{}^{rs}\Gamma^k{}_{rs} - D^k(D_k - 2Z_k) - K^k{}_rK^r{}_k + \mathrm{tr}K(\mathrm{tr}K - 2\Theta)] - 8\pi\alpha\tau. \tag{A16}
$$

## APPENDIX B: FINITE-DIFFERENCES IMPLEMENTATION

We follow the well-known method-of-lines (MoL in [30]) in order to deal separately with the space and the time discretization. Concerning the time discretization, we use the following third-order-accurate Runge-Kutta algorithm

$$
\begin{aligned}
u^* &= u^n + \Delta t\,\mathrm{rhs}(u^n) \\
u^{**} &= \frac{3}{4}u^n + \frac{1}{4}[u^* + \Delta t\,\mathrm{rhs}(u^*)] \\
u^{n+1} &= \frac{1}{3}u^n + \frac{2}{3}[u^{**} + \Delta t\,\mathrm{rhs}(u^{**})],
\end{aligned}
\tag{B1}
$$

which is strong-stability-preserving (SSP in [31]), where we have used as a shorthand

$$\mathrm{rhs}\,(u) \equiv -\partial_k F^k(u) + S(u). \tag{B2}$$

The flux derivatives appearing in (B2) will be discretized by using the finite-difference formula proposed in Ref. [14] (FDOC algorithm). For instance the derivative of $F^x(u)$ will be represented as

$$\partial_x F^x_j = C^{2m}F^x_j + (-1)^m\beta(\Delta x)^{2m}D^m_+ D^{m-1}_-(\lambda_{j-1/2}D_- u_j), \tag{B3}$$

where $C^{2m}$ is the $2m$th-order-accurate central difference operator and $D_\pm$ are the standard finite-difference operators. We have also noted

$$\lambda_{j-1/2} = \max(\lambda_j, \lambda_{j-1}), \tag{B4}$$

where $\lambda_j$ stands here for the local characteristic radius (the highest characteristic speed, typically the gauge speed).

Note that the second term in the finite-difference formula (B3) is actually a dissipation operator of order $2m$ acting on $(\lambda u)$, so it could be regarded at the first sight as a mere generalization of the standard Kreiss-Oliger artificial viscosity operators [32]. This is not the case: the formula (B3) can be instead derived in a finite-volume framework, when combining the local-Lax-Friedrichs flux formula [33] with the (unlimited) Osher-Chakrabarthy flux interpolation [15] (see Ref. [14] for details, including the optimal values of the $\beta$ parameter).

Note that, contrary to the standard Kreiss-Oliger approach, the dissipation term is such that the accuracy of the first (centered derivatives) term in (B3) is reduced by one order: the resulting FDOC algorithm accuracy is always of an odd order. This is important for code robustness. The algorithms (B3) can be shown to keep monotonicity even for remarkably high compression factors (defined as the ratio between two neighbor slopes along a given direction) [14], which is what is actually required in view of the steep profiles shown for instance in Fig. 2.

The space accuracy of the scheme (B3) is $2m - 1$, with an stencil of $2m + 1$ points. We have used in this paper both the third-order and fifth-order accurate methods, for which the optimal values of the dissipation parameter are $\beta = 1/12$, $\beta = 2/75$, respectively [14]. In the fifth-order case, we have a seven-point stencil and the dissipation term corresponds to a sixth derivative, as in the advanced finite-difference schemes used in Ref. [34]. The robustness of the proposed algorithms, with compression factors of 5 and 3, respectively, makes them very convenient for steep-gradient scenarios, such us the ones arising in black-hole simulations, where slice-stretching threatens the stability of more standard finite-difference algorithms [28].

No sophisticated numerical tools (mesh refinement, algorithm-switching for the advection terms, etc.) have been incorporated to our code at this point, when we are facing just test simulations. Concerning the boundary treatment, we simply choose at the points next to the boundary the most accurate centered algorithm compatible with the available stencil there. When it comes to the last point, we can either copy the neighbor value or propagate it out with the maximum propagation speed (by means of a 1D advection equation). The idea is to keep the numerical code as simple as possible in order to test here just the basic algorithm in a clean way.

## APPENDIX C: SCALAR FIELD STUFFING

Let us consider the stress-energy tensor

$$T_{ab} = \Phi_a \Phi_b - 1/2(g^{cd}\Phi_c\Phi_d)g_{ab}, \qquad (C1)$$

where we have noted $\Phi_a = \partial_a \Phi$, corresponding to a scalar field matter content. The $3 + 1$ decomposition of (C1) is given by

$$\tau = 1/2(\Phi_n{}^2 + \gamma^{kl}\Phi_k\Phi_l), \qquad S_i = \Phi_n\Phi_i,$$
$$S_{ij} = \Phi_i\Phi_j + 1/2(\Phi_n{}^2 - \gamma^{kl}\Phi_k\Phi_l)\gamma_{ij}, \qquad (C2)$$

where $\Phi_n$ stands for the normal time derivative:

$$(\partial_t - \beta^k\partial_k)\Phi = -\alpha\Phi_n. \qquad (C3)$$

The quantities (C2) appear as source terms in the field Eqs. (4)–(6).

The stress-energy conservation amounts to the evolution equation for the scalar field, which is just the scalar wave equation. In the $3 + 1$ language, it translates into the flux-conservative form:

$$\partial_t[\sqrt{\gamma}\Phi_n] + \partial_k[\sqrt{\gamma}(-\beta^k\Phi_n + \alpha\gamma^{kj}\Phi_j)] = 0. \qquad (C4)$$

A fully first-order system may be obtained by considering the space derivatives $\Phi_i$ as independent dynamical fields, as we did for the metric space derivatives.

Concerning the initial data, we must solve the energy-momentum constraints. They can be obtained by setting both $\Theta$ and $Z_i$ to zero in (5) and (6). In the time-symmetric case ($K_{ij} = 0$), this amounts to

$$R = 16\pi\tau, \qquad S_i = \Phi_n\Phi_i = 0. \qquad (C5)$$

The momentum constraint will be satisfied by taking $\Phi$ (and then $\Phi_i$) to be zero everywhere on the initial time slice. Concerning the energy constraint, we will consider the line element (31) with $m = m(r)$. We assume a constant mass value $m = M$ for the black-hole exterior, so that the energy constraint in (C5) will be satisfied with $\tau = 0$ there.

In the interior region, the energy constraint will translate instead into the equation

$$m'' = -2\pi r(\Phi_n)^2\left(1 + \frac{m}{2r}\right)^5, \qquad (C6)$$

which can be interpreted as providing the initial $\Phi_n$ value for any convex ($m'' \leq 0$) mass profile. Of course, some regularity conditions both at the center and at the matching point $r_0$ must be assumed. Allowing for (C6), we have taken

$$m = m'' = 0 \qquad (r = 0)$$
$$m = M, \qquad m' = m'' = 0 \qquad (r = r_0).$$

Note that, allowing for (C6), these matching conditions ensure just the continuity of $\Phi_n$, not its smoothness. This can cause some numerical error, as we are currently evolving $\Phi_n$ through the differential Eq. (C4). If this is a problem, we can demand the vanishing of additional derivatives of the mass function $m(r)$, both at the origin and at the matching point (this is actually the case in our shift simulations). This is not required in the standard case ($f = 2/\alpha$, normal coordinates), where we have used a simple profile, with the matching point at the apparent horizon ($r_0 = M/2$), given by

$$m(r) = 4r - 4/M[r^2 + (M/2\pi)^2\sin^2(2\pi r/M)]. \qquad (C7)$$

[1] K. Kiuchi and H-A. Shinkai, Phys. Rev. D **77**, 044010 (2008).
[2] G. Yoneda and H-A. Shinkai, Phys. Rev. D **66**, 124003 (2002).
[3] M. Shibata and Y.-I. Sekiguchi, Phys. Rev. D **72**, 044014 (2005).
[4] M. D. Duez, Y. T. Liu, S. L. Shapiro, and B. C. Stephens, Phys. Rev. D **72**, 024028 (2005).
[5] M. Anderson, E. W. Hirschmann, S. L. Liebling, and D. Neilsen, Classical Quantum Gravity **23**, 6503 (2006).
[6] B. Giacomazzo and L. Rezzolla, Classical Quantum Gravity **24**, S235 (2007).
[7] M. Alcubierre et al., Phys. Rev. D **67**, 084023 (2003).
[8] M. Alcubierre et al., Classical Quantum Gravity **21**, 589 (2004).
[9] N. Jansen, B. Bruegmann, and W. Tichy, Phys. Rev. D **74**, 084022 (2006).
[10] Y. Zlochower, J. G. Baker, M. Campanelli, and C. O. Lousto, Phys. Rev. D **72**, 024021 (2005).
[11] M. Babiuc et al., Classical Quantum Gravity **25**, 125012

(2008).

[12] C. Bona, T. Ledvinka, C. Palenzuela, and M. Žáček, Phys. Rev. D **67**, 104005 (2003).

[13] C. Gundlach, G. Calabrese, I. Hinder, and J. M. Martín-García, Classical Quantum Gravity **22**, 3767 (2005).

[14] C. Bona, C. Bona-Casas, and J. Terradas, J. Comput. Phys. **228**, 2266 (2009); arXiv:0810.2185.

[15] S. Osher and S. Chakravarthy, ICASE Report No. 84-44, ICASE Langley Research Center, Hampton, VA1984.

[16] D. Alic, C. Bona, C. Bona-Casas, and J. Massó, Phys. Rev. D **76**, 104007 (2007).

[17] C. Bona, J. Massó, E. Seidel, and J. Stela, Phys. Rev. Lett. **75**, 600 (1995).

[18] M. Holst *et al.*, Phys. Rev. D **70**, 084017 (2004).

[19] C. Bona, T. Ledvinka, C. Palenzuela, and M. Žáček, Phys. Rev. D **69**, 064036 (2004).

[20] G. Nagy, O. Ortiz, and O. Reula, Phys. Rev. D **70**, 044012 (2004).

[21] C. Bona and J. Massó, Phys. Rev. Lett. **68**, 1097 (1992).

[22] www.appleswithapples.org/TestResults/Results/Abigel05/Abigel05.html.

[23] M. Tiglio, L. Lehner, and D. Neilsen, Phys. Rev. D **70**, 104018 (2004).

[24] L. E. Kidder, M. A. Scheel, and S. A. Teukolsky, Phys. Rev. D **64**, 064017 (2001).

[25] D. Bernstein, Ph. D. thesis, Dept. of Physics, Univ. of Illinois at Urbana-Champaign, 1993.

[26] A. Arbona *et al.*, Phys. Rev. D **57**, 2397 (1998).

[27] A. Arbona, C. Bona, J. Massó, and J. Stela, Phys. Rev. D **60**, 104014 (1999).

[28] B. Reimann and B. Bruegmann, Phys. Rev. D **69**, 044006 (2004).

[29] C. Bona and C. Palenzuela, Phys. Rev. D **69**, 104003 (2004).

[30] O. A. Liskovets, J. Diff. Eq. **1**, 1308 (1965).

[31] C.-W. Shu and S. Osher, J. Comput. Phys. **77** 439 (1988).

[32] B. Gustafsson, H. O. Kreiss, and J. Oliger, *Time Dependent Problems and Difference Methods* (Wiley-Interscience, New York, 1995).

[33] V. V. Rusanov, J. Comput. Math. Phys. USSR **1**, 267 (1961).

[34] S. Husa *et al.*, Classical Quantum Gravity **25**, 105006 (2008).